Japanese Journal of Applied Physics
Vol. 47, No. 5, 2008, pp. 4180–4187

Threshold Setting for Likelihood Function for Elasticity-Based Tissue Classification of Arterial Walls by Evaluating Variance in Measurement of Radial Strain

Kentaro TSUZUKI, Hideyuki HASEGAWA, Hiroshi KANAI*, Masataka ICHIKI[1], and Fumiaki TEZUKA[2]

Graduate School of Engineering, Tohoku University, Sendai 980-8579, Japan
[1]*Sendai Hospital of East Railway Company, Sendai 983-8508, Japan*
[2]*Sendai Medical Center, Sendai 980-8520, Japan*

(Received November 26, 2007; revised February 20, 2008; accepted March 3, 2008; published online May 23, 2008)

Pathologic changes in arterial walls significantly influence their mechanical properties. We have developed a correlation-based method, the *phased tracking method* [H. Kanai *et al.*: IEEE Trans. Ultrason. Ferroelectr. Freq. Control **43** (1996) 791], for measurement of the regional elasticity of the arterial wall. Using this method, elasticity distributions of lipids, blood clots, fibrous tissue, and calcified tissue were measured *in vitro* by experiments on excised arteries (mean ± SD: lipids 89 ± 47 kPa, blood clots 131 ± 56 kPa, fibrous tissue 1022 ± 1040 kPa, calcified tissue 2267 ± 1228 kPa) [H. Kanai *et al.*: Circulation **107** (2003) 3018; J. Inagaki *et al.*: Jpn. J. Appl. Phys. **44** (2005) 4593]. It was found that arterial tissues can be classified into soft tissues (lipids and blood clots) and hard tissues (fibrous tissue and calcified tissue) on the basis of their elasticity. However, there are large overlaps between elasticity distributions of lipids and blood clots and those of fibrous tissue and calcified tissue. Thus, it was difficult to differentiate lipids from blood clots and fibrous tissue from calcified tissue by simply thresholding elasticity value. Therefore, we previously proposed a method by classifying the elasticity distribution in each region of interest (ROI) (not a single pixel) in an elasticity image into lipids, blood clots, fibrous tissue, or calcified tissue based on a likelihood function for each tissue [J. Inagaki *et al.*: Jpn. J. Appl. Phys. **44** (2006) 4732]. In our previous study, the optimum size of an ROI was determined to be 1,500 μm in the arterial radial direction and 1,500 μm in the arterial longitudinal direction [K. Tsuzuki *et al.*: Ultrasound Med. Biol. **34** (2008) 573]. In this study, the threshold for the likelihood function used in the tissue classification was set by evaluating the variance in the ultrasonic measurement of radial strain. The recognition rate was improved from 50 to 54% by the proposed thresholding. [DOI: 10.1143/JJAP.47.4180]

KEYWORDS: atherosclerosis, phased tracking method, radial strain, tissue classification

1. Introduction

Noninvasive measurement of mechanical properties of the arterial wall, such as elasticity, is useful for diagnosis of atherosclerosis because there are significant differences between the elastic moduli of normal arterial walls and those affected by atherosclerosis.[1–3] In particular, mechanical properties of plaque are important because the rupture of plaque may cause acute myocardial infarction and cerebral infarction.[4–6] Magnetic resonance imaging (MRI) and intravascular ultrasound (IVUS) are promising technologies for directly imaging plaque morphology,[7,8] but they are expensive or invasive. On the other hand, the dynamic change of artery diameter due to the pulsation of the heart can be measured noninvasively by methods using ultrasound.[9–12] Some parameters related to artery-wall elasticity can be obtained by the measured change in diameter of the artery.[13–15] However, in the derivation of these parameters, the artery is assumed to be a cylindrical shell with uniform wall thickness and homogeneous elasticity and, thus, the regional elasticity around atherosclerotic plaques cannot be evaluated.

For the measurement of the mechanical properties of the arterial wall, including walls with atherosclerotic plaques, we have developed a method, the *phased tracking method*, for measuring small vibrations in the heart wall or arterial wall with transcutaneous ultrasound.[16,17] For some years, we have measured the displacement and small change in thickness of the arterial wall caused by the heartbeat using this method.[18–21] In our *phased tracking method*, a set of two points is assigned along an ultrasonic beam, and the change in thickness of the layer between these two points is estimated. Furthermore, by sliding the position of the layer along the ultrasonic beam by intervals of the sampled points, the spatial distribution of changes in thickness along the ultrasonic beam can be obtained.

Elasticity images of the human carotid artery have been obtained noninvasively by the measured displacement distribution, and the potential for transcutaneous tissue characterization has been shown by classifying elasticity images using elasticity reference data obtained from *in-vitro* experiments.[21–23]

We have already measured the elasticity distributions for lipids, blood clots, fibrous tissue (mixture of the smooth muscle and collagen), and calcified tissue. In these previous studies, it was found that arterial tissues can be classified into soft tissues (lipids, blood clots) and hard tissues (fibrous tissue, calcified tissue) on the basis of their elasticity. However, it was difficult to differentiate lipids from blood clots and fibrous tissue from calcified tissue because there are large overlaps between their elasticity distributions. Therefore, we proposed a tissue classification method using the elasticity distribution in a small region.[24] In this method, the elasticity distribution of each small ROI (not a single pixel) in an elasticity image was used to classify the ROI into lipids, blood clots, fibrous tissue, or calcified tissue, which improved the precision of tissue classification.

To optimize tissue classification, some parameters have been investigated. In our previous study, the optimum size of an ROI was determined to be 1,500 μm in the arterial radial direction and 1,500 μm in the arterial longitudinal direction.[25] In addition, in the proposed classification method, the likelihood function of each small ROI is calculated for each tissue component (lipids, blood clots, fibrous tissue, and calcified tissue), and the region is classified into the tissue component that has the maximum likelihood.[24] Every ROI is always classified into one of the four tissue components

*E-mail address: hkanai@ecei.tohoku.ac.jp

even when its maximum likelihood is very small. However, such a region should be defined as "an unclassified region" by setting a threshold for the maximum likelihood. In this study, the threshold for the likelihood was set by evaluating the variance in the ultrasonic measurement of radial strain. Tissue classification was much improved by the proposed thresholding in comparison with that in the previous study.

2. Methods

2.1 *Tissue classification based on elasticity distribution measured by ultrasound*

The elasticity of the arterial wall is defined as the tissue strain calibrated by the average stress of the entire wall thickness, namely, the circumferential elastic modulus E_θ^h.[22] The strain distribution is obtained by applying the *phased tracking method* to the measured demodulated signals.[20,26]

In this study, each pixel in an elasticity image was classified into one of five categories, lipids, blood clots, fibrous tissue, calcified tissue, or unclassified, using the likelihood function L_i ($i = 1$: lipids, 2: blood clots, 3: fibrous tissue, 4: calcified tissue) of the elasticity distribution in the small region around the pixel. To obtain the likelihood function L_i, the elasticity distribution of the i-th tissue was translated into the normal distribution to describe the probability distribution using the mean and the standard deviation.[24]

For example, the elasticity distribution of fibrous tissue was translated into the normal distribution as shown in Fig. 1. From *in-vitro* experiments, the elasticity distribution of each tissue i was obtained as illustrated in Fig. 1(a). The elasticity distribution of the i-th tissue is composed of J_i data points with the respective elastic moduli. Using all data of J_i points (J_1: 228, J_2: 179, J_3: 19,121, J_4: 1,101) with the respective elastic moduli, the ascending sequence was constructed for tissue i as shown in Fig. 1(b). In this sequence, the j-th data point ($j = 1, 2, \ldots, J_i$) has the corresponding elastic modulus E_j ($E_j \leq E_{j+1}$), where j is the elasticity number. The probability distribution of each tissue was obtained by allocating all the data of J_i points of each tissue i to boxes of the normal distribution. The box numbers, B_i, of the normal distribution were determined so that the number of data points in the box at each end was only one. As shown in Fig. 1(c), the number of data points, $D_{i,h}$ ($h = 1, 2, \ldots, B_i$) included in box B_i was determined to follow the profile of the normal distribution. Thus, the $(J_i/2)$-th data point was included in the box with the highest probability. By allocating all the data of J_i points of each tissue to boxes of the corresponding normal distribution, the mean elasticity of the data included in each box was obtained.

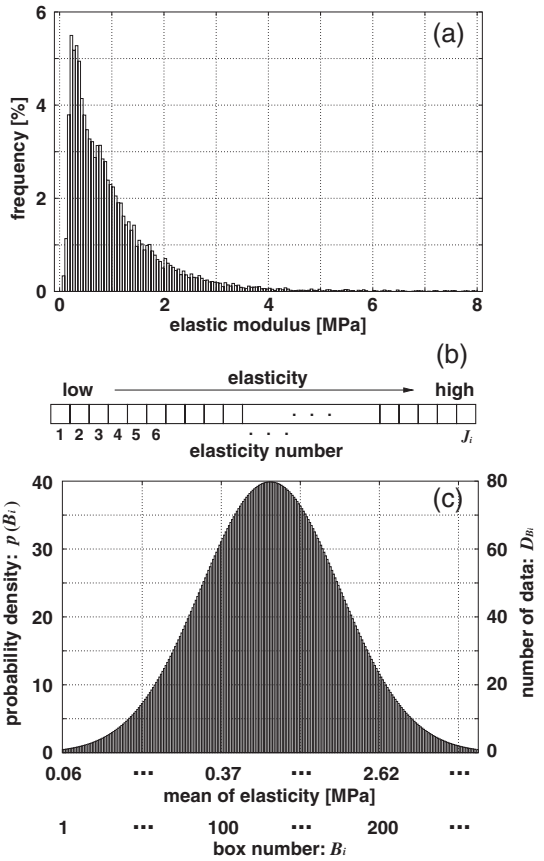

Fig. 1. (a) Original elasticity distribution of the tissue. (b) Ascending sequence of elastic modulus in an elasticity distribution. (c) Normal distribution. The number of boxes in which depends on the number of data points in (a).

As shown in Fig. 2, an ROI was assigned to an elasticity image which was obtained by ultrasonic measurement. The likelihood function $L_i(m, n)$ is defined as a joint probability that all the elasticity values in ROI $R_{m,n}$ (center of ROI: n-th sampled point along m-th beam) simultaneously belong in the i-th category as follows:

$$L_i(m,n) = \left(\prod_{(k,l)\in R_{m,n}} p_i(E_{k,l}) \right)^{1/N_0}, \quad (i = 1,2,3,4) \qquad (2.1)$$

where $p_i(E_{k,l})$ is the probability density that elasticity value $E_{k,l}$ in the k-th row and l-th column in the $R_{m,n}$ belongs to the

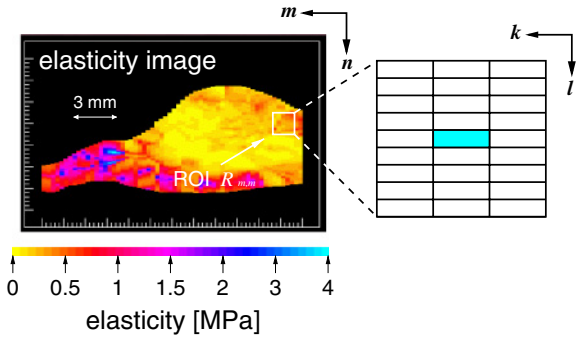

Fig. 2. (Color online) Illustration of a ROI.

i-th tissue category, and N_0 denotes the number of pixels in $R_{m,n}$. The number of pixels in the ROI near the boundary of the elasticity image is less than that in the ROI which is sufficiently away from the boundary. Thus, the geometric mean $1/N_0$ is used to compensate for the size N_0 of the ROI. The pixel at the center of the ROI is classified into the class which has the maximum likelihood.

In this classification, there may be a region which has an extremely small value for the maximum likelihood. Such regions are classified into the unclassified region by setting the threshold $T_{o,i}(R_{m,n})$ to the maximum likelihood. Thus, the category $C(R_{m,n})$, to which an ROI $R_{m,n}$ belongs, is expressed as follows:

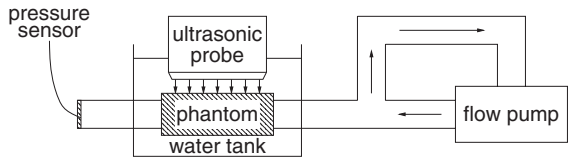

Fig. 3. Schematic diagram of the phantom experimental system.

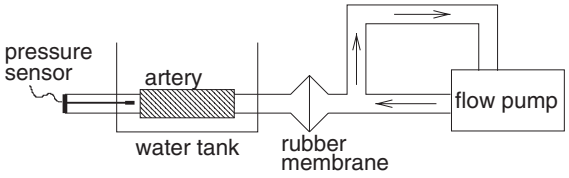

Fig. 4. Schematic diagram of the *in-vitro* experimental system.

$$C(R_{m,n}) = \begin{cases} \arg\max\limits_{1\le i\le 4} L_i(m,n) & \text{if } \max\limits_{1\le i\le 4} L_i(m,n) \ge T_{\mathrm{o},i}(R_{m,n}), \\ \text{unclassified} & \text{otherwise.} \end{cases} \tag{2.2}$$

In this study, arterial tissue was classified into one of four classes, lipids, blood clots, fibrous tissue, and calcified tissue. A normal arterial wall is composed mainly of smooth muscle and collagen. Atherosclerosis changes the contents of these tissue components, and it is difficult to determine what contents of these components are abnormal. Therefore, in this study, a tissue composed of smooth muscle and collagen was defined as a class, namely, fibrous tissue.

2.2 *Phantom experiment for evaluation of variance in measurement of radial strain*

Figure 3 shows the experimental setup for the phantom experiment. A homogeneous cylindrical phantom (internal radius: $r_\mathrm{i} = 4\,\mathrm{mm}$, external radius: $r_\mathrm{o} = 5\,\mathrm{mm}$, elastic modulus: $E = 750\,\mathrm{kPa}$) made from silicone rubber containing 5% carbon powder by weight was measured with a 7.5 MHz linear ultrasonic probe. The scan plane was parallel to the longitudinal direction of the phantom, and the directions of all ultrasonic beams coincided with the radial direction of the phantom. The change in internal pressure, which was applied using a flow pump, was measured by a pressure sensor. The sampling frequency of the quadrature demodulated signal and the frame rate are 10 MHz and 200 Hz, respectively. The theoretical value of radial strain $\Delta\varepsilon_\mathrm{r}(r)$ at each radial position r is obtained by[27]

$$\Delta\varepsilon_\mathrm{r}(r) = -\frac{3}{2}\frac{r_\mathrm{i}^2 r_\mathrm{o}^2}{(r_\mathrm{o}^2 - r_\mathrm{i}^2)r^2}\frac{\Delta p}{E}, \tag{2.3}$$

where Δp is the pressure increment. The radial strain measured by the *phased tracking method* was compared with the theoretical value $\Delta\varepsilon_\mathrm{r}(r)$.

2.3 *In-vitro experiment for tissue classification of arterial wall*

Figure 4 shows a schematic diagram of the measurement system. The change in pressure inside the artery was realized by circulating fluid using a flow pump. The fluid inside the artery and that circulating in the flow pump were separated by a rubber membrane to prevent the flow pump from being contaminated, and only the change in internal pressure was propagated to the inside of the artery. The change in internal pressure was measured by a pressure transducer (Camino Model 110-4).

In ultrasonic measurements, excised arteries were measured with a conventional 7.5 MHz linear ultrasonic probe (Toshiba SSH-140A). The quadrature demodulated signals of RF echoes were acquired at 10 MHz at a frame rate of 200 Hz.

3. Results

3.1 *Phantom experiments for evaluation of variance in strain measurement*

Figures 5(a)–5(d) show the strain distribution along the radial direction of the phantom obtained by the *phased tracking method* for cases of pressure increments $\Delta p = 40$, 50, 60, and 70 mmHg, respectively. Plots and vertical bars show means and standard deviations for 60 ultrasonic beams. The standard deviation and the difference between the mean and the theoretical value at each applied pressure increment are shown in Table I. In Table I, the variance in measurement of radial strain was almost constant even when the magnitude of the pressure increment Δp varied. Moreover, the difference between the mean and the theoretical value is lower than the standard deviation, and mean value follows the theoretical profile.

Figure 6 shows the relationship between the mean μ_s and the standard deviation σ_s normalized by the mean value. The plots and the straight line show all the measured results in Fig. 5 and the regression line, respectively. A positive correlation was found between the mean μ_s and the normalized standard deviation σ_s because the standard deviation was almost constant over every pressure increment. The regression line was determined as follows:

$$\sigma_\mathrm{s} = 0.071\mu_\mathrm{s} + 0.40. \tag{3.1}$$

3.2 *Setting threshold in tissue classification*

Figure 7 shows the elasticity distribution of each tissue; that is, the frequency of the elasticity values which belong to the range is defined by the position and width of each vertical bar. The width of a vertical bar was set at every 50 kPa. Means and the standard deviations are 89 ± 47 (lipids), 131 ± 56 (blood clots), $1{,}022 \pm 1{,}040$ (fibrous tissue), and $2{,}267 \pm 1{,}228$ kPa (calcified tissue). Although similarities were found in the elasticity distributions of lipids and blood clots and in those of fibrous and calcified tissues, there are differences in the elasticity distributions of these tissues.

Figure 8 shows the probability density of each tissue obtained by the axis transformation of the elasticity distribution using the process described in §2.1. As shown in these figures, the horizontal axis of the elastic modulus is nonlinear. Using these databases, each pixel in an elasticity image was classified as a certain tissue component.

The threshold $T_{\mathrm{o},i}(R_{m,n})$ for likelihood function $L_i(m,n)$ of tissue i of each ROI $R_{m,n}$ is determined using the experimental results with the phantom. Using eq. (3.1), the normalized standard deviation $\sigma_\mathrm{s}(R_{m,n})$ in the measurement of the radial strain in $R_{m,n}$ was given approximately by:

$$\sigma_\mathrm{s}(R_{m,n}) = 0.071\bar{\mu} + 0.40, \tag{3.2}$$

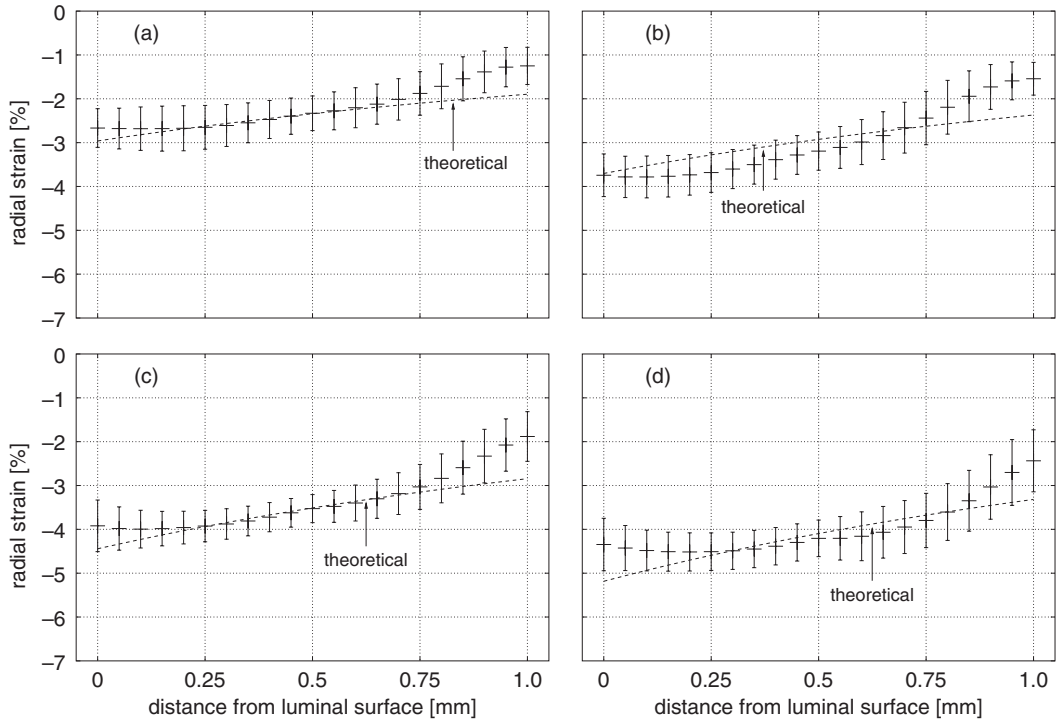

Fig. 5. Measured radial strain distribution along the radial axis of a cylindrical phantom: $\Delta p =$ (a) 40, (b) 50, (c) 60, and (d) 70 mmHg.

Table I. The standard deviation of radial strain and average of the difference between the mean and the theoretical value.

Pressure Δp (mmHg)	Standard deviation (%)	Difference (%)
40	0.47	0.19
50	0.49	0.35
60	0.45	0.23
70	0.54	0.29

$$\bar{\mu} = \frac{1}{N_0} \sum_{(k,l)\in R_{m,n}} \varepsilon_{\max}(k,l), \tag{3.3}$$

where $\varepsilon_{\max}(k,l)$ and $\bar{\mu}$ are the maximum radial strain during one cardiac cycle in the k-th row and l-th column and the average of the maximum radial strain in $R_{m,n}$, respectively.

Figure 9 shows an illustration for determining the threshold $T_{o,i}(R_{m,n})$ for the likelihood function $L_i(m,n)$ of tissue i. Let us consider the elasticity distribution in an ROI. Variance $\sigma_0^2(R_{m,n})$ of the measured elasticity $\widehat{E}_{k,l}$ in the k-th row and l-th column in $R_{m,n}$ is expressed as follows:

$$\begin{aligned}
\sigma_0^2(R_{m,n}) &= \mathop{\mathrm{E}}_{(k,l)\in R_{m,n}}\left[\left(\widehat{E}_{k,l} - \mathop{\mathrm{E}}_{(k,l)\in R_{m,n}}[\widehat{E}_{k,l}]\right)^2\right] \\
&= \mathop{\mathrm{E}}_{(k,l)\in R_{m,n}}\left[\left(\widehat{E}_{k,l} - \overline{\widehat{E}}_{R_{m,n}}\right)^2\right] \\
&= \mathop{\mathrm{E}}_{(k,l)\in R_{m,n}}\left[\widehat{E}_{k,l}^2 - 2\widehat{E}_{k,l}\cdot\overline{\widehat{E}}_{R_{m,n}} + \left(\overline{\widehat{E}}_{R_{m,n}}\right)^2\right] \\
&= \mathop{\mathrm{E}}_{(k,l)\in R_{m,n}}\left[\widehat{E}_{k,l}^2\right] - \left(\overline{\widehat{E}}_{R_{m,n}}\right)^2,
\end{aligned} \tag{3.4}$$

where $\mathrm{E}_{(k,l)\in R_{m,n}}[\cdot]$ shows the averaging for the data included in the ROI $R_{m,n}$, and $\overline{\widehat{E}}_{R_{m,n}}$ is the average of the measured elasticity values $\{\widehat{E}_{k,l}\}$ in $R_{m,n}$. By assuming that the true elasticity values $\{E_{k,l}\}$ are not constant in $R_{m,n}$ due to the elasticity inhomogeneity of tissue even when there is no measurement error, the measured elasticity $\{\widehat{E}_{k,l}\}$ is described by the sum of true elasticity $\{E_{k,l}\}$ and the error $\{\Delta E_{k,l}\}$ (sum of random error $\{e_{k,l}\}$ and bias error $b_{R_{m,n}}$) as follows:

$$\widehat{E}_{k,l} = E_{k,l} + \Delta E_{k,l}. \quad (k,l) \in R_{m,n} \tag{3.5}$$

Thus, the mean $\overline{\widehat{E}}_{R_{m,n}}$ of the measured elasticity values $\{\widehat{E}_{k,l}\}$ is given by

$$\begin{aligned}
\overline{\widehat{E}}_{R_{m,n}} &= \mathop{\mathrm{E}}_{(k,l)\in R_{m,n}}[\widehat{E}_{k,l}] \\
&= \mathop{\mathrm{E}}_{(k,l)\in R_{m,n}}[E_{k,l} + \Delta E_{k,l}] \\
&= \mathop{\mathrm{E}}_{(k,l)\in R_{m,n}}[E_{k,l}] + b_{R_{m,n}} \\
&= \overline{E}_{R_{m,n}} + b_{R_{m,n}},
\end{aligned} \tag{3.6}$$

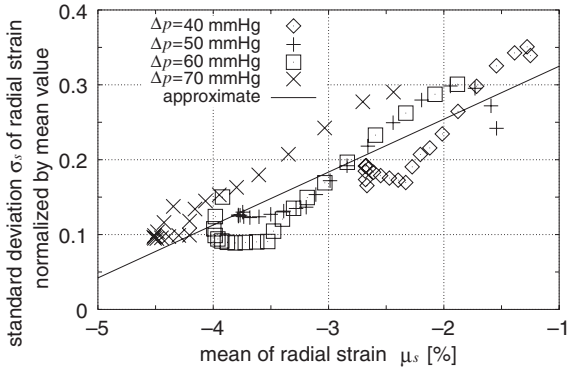

Fig. 6. Relationship between the mean and the normalized standard deviation σ_s of radial strain.

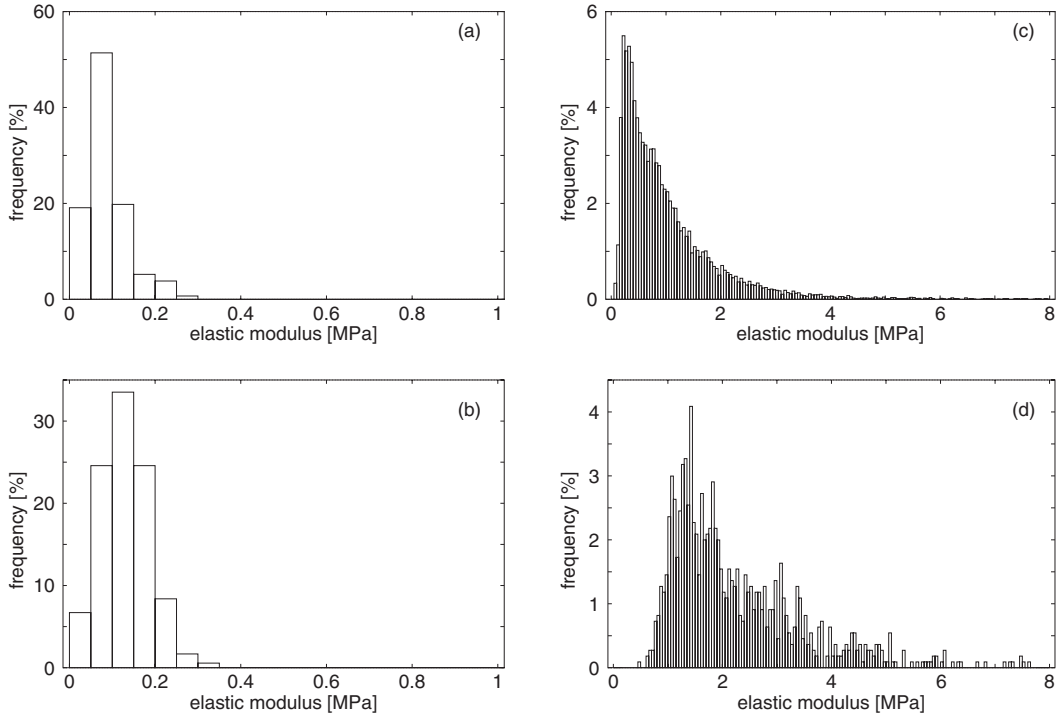

Fig. 7. Elasticity distribution of each tissue. (a) Lipids ($N = 288$). (b) Blood clots ($N = 178$). (c) Fibrous tissue ($N = 19{,}120$). (d) Calcified tissue ($N = 1{,}101$).

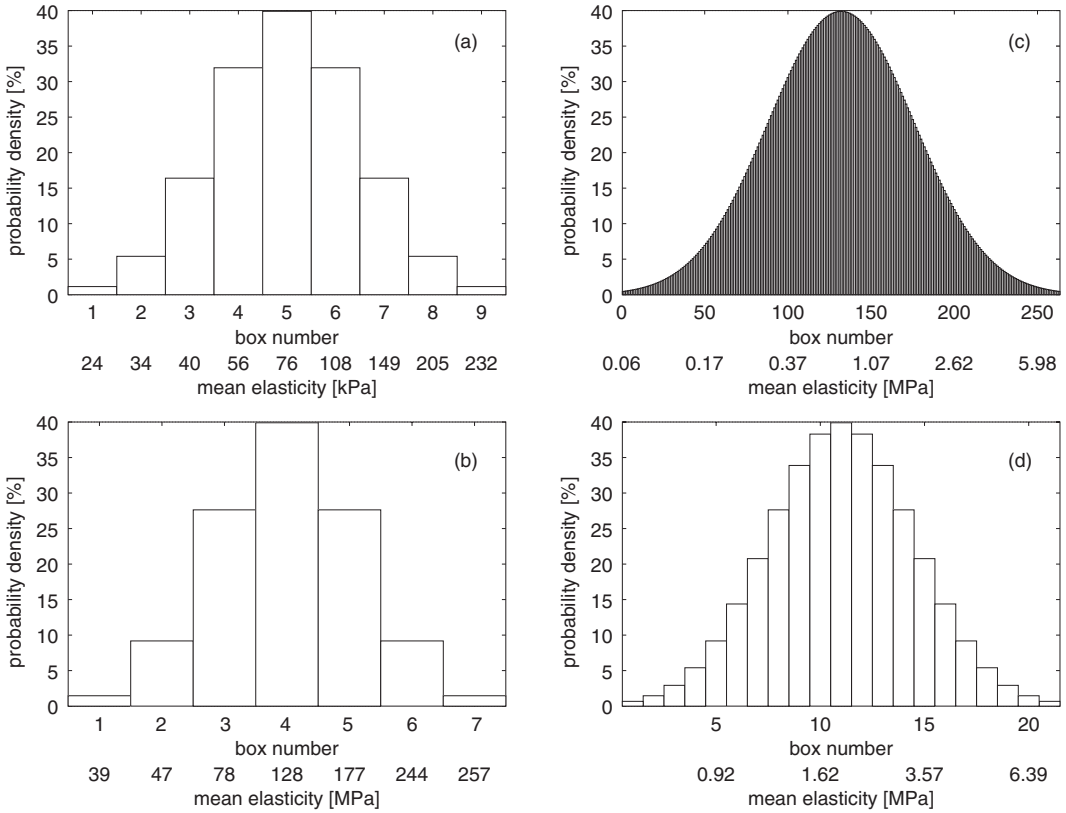

Fig. 8. Probability density for each tissue. (a) Lipids. (b) Blood clots. (c) Fibrous tissue. (d) Calcified tissue.

where $\overline{E}_{R_{m,n}}$ and $b_{R_{m,n}}$ are the true mean elasticity in $R_{m,n}$ and the bias error $b_{R_{m,n}} = \mathrm{E}_{(k,l)\in R_{m,n}}[\Delta E_{k,l}]$, respectively. By substituting eq. (3.6), eq. (3.4) is modified as follows:

$$\begin{aligned}
\sigma_0^2(R_{m,n}) &= \mathop{\mathrm{E}}_{(k,l)\in R_{m,n}}\left[(E_{k,l}+\Delta E_{k,l})^2\right] - (\overline{E}_{R_{m,n}} + b_{R_{m,n}})^2 \\
&= \mathop{\mathrm{E}}_{(k,l)\in R_{m,n}}[E_{k,l}^2] + 2\mathop{\mathrm{E}}_{(k,l)\in R_{m,n}}[E_{k,l}\cdot\Delta E_{k,l}] + \mathop{\mathrm{E}}_{(k,l)\in R_{m,n}}[\Delta E_{k,l}^2] - (\overline{E}_{R_{m,n}} + b_{R_{m,n}})^2 \\
&= \mathop{\mathrm{E}}_{(k,l)\in R_{m,n}}[E_{k,l}^2] + 2\mathop{\mathrm{E}}_{(k,l)\in R_{m,n}}[E_{k,l}\cdot e_{k,l}] + 2b_{R_{m,n}}\mathop{\mathrm{E}}_{(k,l)\in R_{m,n}}[E_{k,l}] + \mathop{\mathrm{E}}_{(k,l)\in R_{m,n}}[\Delta E_{k,l}^2] - (\overline{E}_{R_{m,n}} + b_{R_{m,n}})^2 \\
&= \mathop{\mathrm{E}}_{(k,l)\in R_{m,n}}[E_{k,l}^2] + 2\mathop{\mathrm{E}}_{(k,l)\in R_{m,n}}[E_{k,l}\cdot e_{k,l}] + 2b_{R_{m,n}}\mathop{\mathrm{E}}_{(k,l)\in R_{m,n}}[E_{k,l}] + \mathop{\mathrm{E}}_{(k,l)\in R_{m,n}}\left[(e_{k,l}+b_{R_{m,n}})^2\right] - (\overline{E}_{R_{m,n}} + b_{R_{m,n}})^2 \\
&= \mathop{\mathrm{E}}_{(k,l)\in R_{m,n}}[E_{k,l}^2] + 2\mathop{\mathrm{E}}_{(k,l)\in R_{m,n}}[E_{k,l}\cdot e_{k,l}] + 2b_{R_{m,n}}\mathop{\mathrm{E}}_{(k,l)\in R_{m,n}}[E_{k,l}] + \mathop{\mathrm{E}}_{(k,l)\in R_{m,n}}[e_{k,l}^2] \\
&\quad + 2b_{R_{m,n}}\mathop{\mathrm{E}}_{(k,l)\in R_{m,n}}[e_{k,l}] + b_{R_{m,n}}^2 - (\overline{E}_{R_{m,n}} + b_{R_{m,n}})^2 \\
&= \mathop{\mathrm{E}}_{(k,l)\in R_{m,n}}[E_{k,l}^2] - \overline{E}_{R_{m,n}}^2 + \mathop{\mathrm{E}}_{(k,l)\in R_{m,n}}\left[(e_{k,l}-\overline{e}_{R_{m,n}})^2\right] + 2\mathop{\mathrm{E}}_{(k,l)\in R_{m,n}}[E_{k,l}\cdot e_{k,l}] + 2b_{R_{m,n}}\mathop{\mathrm{E}}_{(k,l)\in R_{m,n}}[e_{k,l}] \\
&= \mathop{\mathrm{E}}_{(k,l)\in R_{m,n}}\left[\left(E_{k,l} - \mathop{\mathrm{E}}_{(k,l)\in R_{m,n}}[E_{k,l}]\right)^2\right] + \mathop{\mathrm{E}}_{(k,l)\in R_{m,n}}\left[(e_{k,l}-\overline{e}_{R_{m,n}})^2\right] + 2\mathop{\mathrm{E}}_{(k,l)\in R_{m,n}}[E_{k,l}\cdot e_{k,l}] + 2b_{R_{m,n}}\mathop{\mathrm{E}}_{(k,l)\in R_{m,n}}[e_{k,l}], \qquad (3.7)
\end{aligned}$$

where $\overline{e}_{R_{m,n}}$ is assumed to be zero because $\{e_{k,l}\}$ is random error. Variance $(\sigma_e(R_{m,n}))^2$ of the measurement error $\{e_{k,l}\}$ in $R_{m,n}$ is expressed by $(\sigma_e(R_{m,n}))^2 = (\sigma_s(R_{m,n})\cdot\widehat{\overline{E}}_{R_{m,n}})^2$, where $\sigma_s(R_{m,n})$ is determined by eq. (3.2). By defining the variance due to the elastic inhomogeneity of tissue in $R_{m,n}$ by $\sigma(R_{m,n})^2$, eq. (3.7) is expressed as follows:

$$\sigma_0^2(R_{m,n}) = (\sigma(R_{m,n}))^2 + \left(\sigma_s(R_{m,n})\cdot\widehat{\overline{E}}_{k,l}\right)^2 + 2\mathop{\mathrm{E}}_{(k,l)\in R_{m,n}}[E_{k,l}\cdot e_{k,l}], \qquad (3.8)$$

where there is no correlation between the inhomogeneity of $E_{k,l}$ and $\{e_{k,l}\}$ in $R_{m,n}$. Therefore, variance $(\sigma(R_{m,n}))^2$ without error of eq. (3.8) is given by $\{\sigma_s(R_{m,n})\widehat{\overline{E}}_{R_{m,n}}\}^2$ subtracted from the variance σ_0^2 of the measured elasticity values $\{\widehat{E}_{k,l}\}$ in $R_{m,n}$ as follows:

$$(\sigma(R_{m,n}))^2 = \sigma_0^2 - \left\{\sigma_s(R_{m,n})\widehat{\overline{E}}_{R_{m,n}}\right\}^2. \qquad (3.9)$$

Based on this relation, by setting the acceptance region [from $\mu_i - a\sigma_i(R_{m,n})$ to $\mu_i + a\sigma_i(R_{m,n})$] of the probability density $N(\mu_i, \sigma_i^2(R_{m,n}))$ for each tissue i, the threshold $T_{o,i}(R_{m,n})$ for the likelihood function $L_i(m,n)$ of tissue i in $R_{m,n}$ was determined by the probability of the distribution $N(\mu_i, \sigma_{0,i}^2(R_{m,n}))$ with the error at the distance from mean μ_i as shown in Fig. 9. Therefore, the threshold $T_{o,i}(R_{m,n})$ for the likelihood function $L_i(m,n)$ of tissue i is given by

$$T_{o,i}(R_{m,n}) = \frac{1}{\sqrt{2\pi}\sigma_{0,i}}\exp\left[-\frac{\left(a\sqrt{\sigma_0^2(R_{m,n}) - \left\{\sigma_s(R_{m,n})\widehat{\overline{E}}_{R_{m,n}}\right\}^2}\right)^2}{2\sigma_{0,i}^2}\right], \qquad (3.10)$$

where $\sigma_{0,i}$ is the variance of measured elasticity distribution for tissue i.

Let us define the ratio of the area of the acceptance region $\mu_i \pm a\sigma_i(R_{m,n})$ in the normal distribution $N(\mu_i, \sigma_i^2(R_{m,n}))$ to the entire area of $N(\mu_i, \sigma_i^2(R_{m,n}))$ by w. Figure 10 shows an example of a tissue classification image that is estimated manually by referring to its pathologic image. By comparing the pathology-based classification image shown in Fig. 10 with the tissue classification image obtained by the proposed method, the number $N_c(w)$ of correctly classified pixels is obtained. The recognition rate $R_r(w)$ at w is expressed as follows:

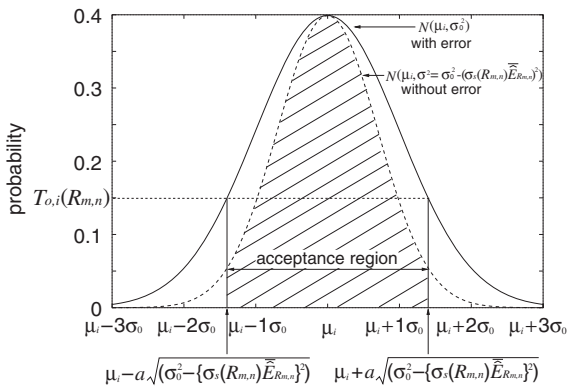

Fig. 9. Illustration for determining the threshold $T_{o,i}(R_{m,n})$ for the likelihood function $L_i(m,n)$.

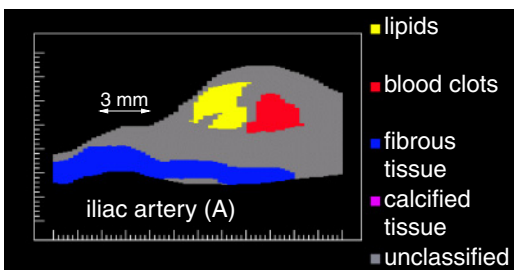

Fig. 10. (Color online) Tissue classification image obtained by referring to the pathologic image.

$$R_r(w) = \frac{N_c(w)}{N_{all}(w)} \times 100\ (\%), \tag{3.11}$$

where $N_{all}(w)$ is the number of all pixels classified into a class except for an unclassified pixel. Figure 11 shows the relationship between the area ratio w of the acceptance region and the recognition rate $R_r(w)$ obtained using eight iliac arteries and nine femoral arteries. By setting the threshold $T_{o,i}(S_{ROI})$ ($w \leq 99\%$), the recognition rate $R_r(w)$ was increased compared with that at $w = 100\%$ (without thresholding) and the recognition rate $R_r(w)$ slightly was increased by decreasing the area ratio w of the acceptance region at the expense of the number of classified pixels.

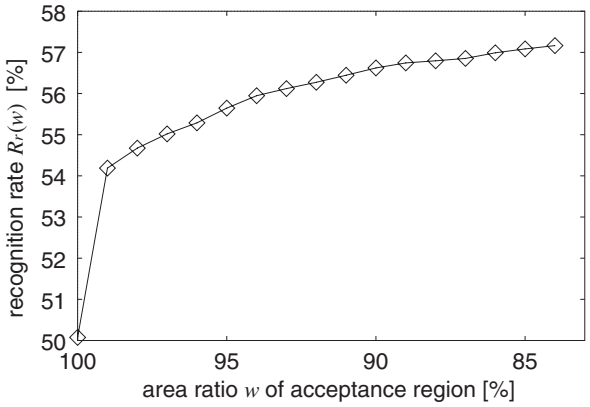

Fig. 11. Relationship between the area ratio w of the acceptance region and the recognition rate $R_r(w)$.

Figures 12(c)–12(g) show the tissue classification images for an excised human iliac artery (A). The regions classified as lipids, blood clots, fibrous tissue, and calcified tissue are color-coded yellow, red, blue, and purple, respectively. Figure 12(c) shows the classification image obtained with an ROI size of 5×20 pixels ($1{,}500 \times 1{,}500\,\mu m^2$) without thresholding. Although the pixels were roughly classified into the correct tissues, the pixels which have low likelihood $L_i(m,n)$ were also classified. Figures 12(d)–12(g) show the classification images obtained with thresholds $T_{o,i}(R_{m,n})$ determined at four different area ratios of $w = 99$, 95, 90, and 85%, respectively. In Figs. 12(d)–12(g), a region whose likelihood is less than the threshold $T_{o,i}(R_{m,n})$ for all tissue components is colored gray. As shown in Figs. 12(d)–12(g), similarities among the classification images seem to be qualitatively high especially for those at an area ratio w less than or equal to 95%. It can be expected from the result shown in Fig. 11 that improvement in the recognition rate $R_r(w)$ by decreasing area ratio w slightly diminish at area ratio w less than 95%. For another specimen [iliac artery (B)], some pixels were misclassified into blood clots or calcified tissue when the threshold $T_{o,i}(R_{m,n})$ was not set, as shown in Fig. 13(c). In Figs. 13(d)–13(g), by setting $w \leq 95\%$, the pixels misclassified in the blood clots were classified into unclassified region. For these results, the

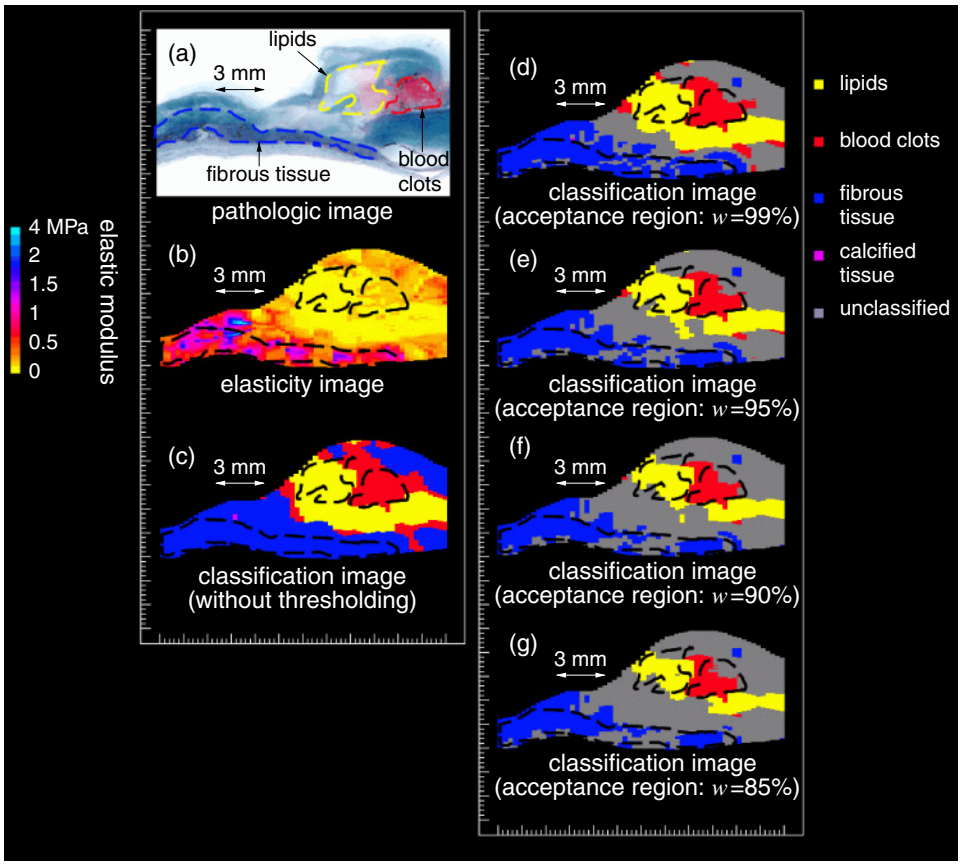

Fig. 12. (Color online) Iliac artery (A): (a) Pathologic image subjected to elastica-Masson staining. (b) Elasticity image. (c) Tissue classification image without thresholding. (d) Tissue classification image ($w = 99\%$). (e) Tissue classification image ($w = 95\%$). (f) Tissue classification image ($w = 90\%$). (g) Tissue classification image ($w = 85\%$).

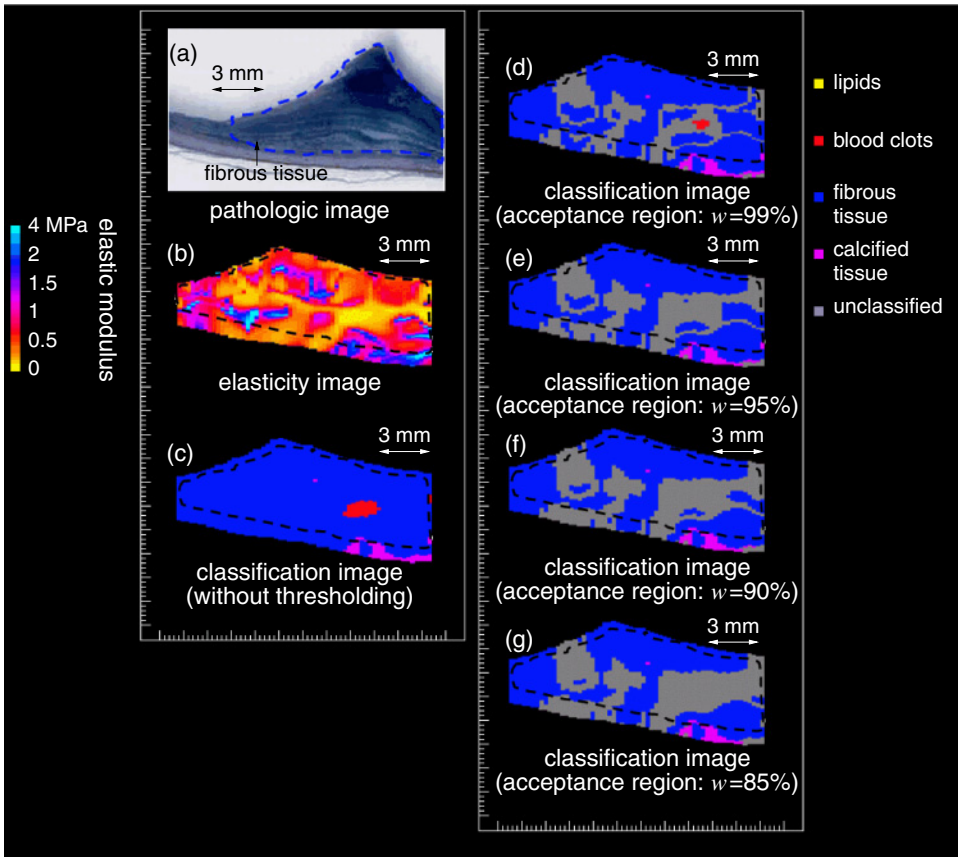

Fig. 13. (Color online) Iliac artery (B): (a) Pathologic image subjected to elastica-Masson staining. (b) Elasticity image. (c) Tissue classification image without thresholding. (d) Tissue classification image ($w = 99\%$). (e) Tissue classification image ($w = 95\%$). (f) Tissue classification image ($w = 90\%$). (g) Tissue classification image ($w = 85\%$).

misclassification was reduced using the threshold $T_{o,i}(R_{m,n})$ determined from the area ratio of the acceptance region less than or equal to 95%.

4. Conclusions

In this study, variance in measured radial strain was evaluated to set the threshold $T_{o,i}(R_{m,n})$ for the likelihood $L_i(m,n)$ used in elasticity-based tissue classification of the arterial wall. The misclassification was reduced using the threshold $T_{o,i}(R_{m,n})$ determined by setting the area ratio of the acceptance region less than or equal to 95%.

1) R. T. Lee, A. J. Grodzinsky, E. H. Frank, R. D. Kamm, and F. J. Schoen: Circulation **83** (1991) 1764.
2) H. M. Loree, A. J. Grodzinsky, S. Y. Park, L. J. Gibson, and R. T. Lee: J. Biomech. **27** (1994) 195.
3) P. C. G. Simons, A. Algra, M. L. Bots, D. E. Grobbee, and Y. van der Graaf: Circulation **100** (1999) 951.
4) E. Falk, P. K. Shah, and V. Fuster: Circulation **92** (1995) 657.
5) M. J. Davies: Circulation **94** (1996) 2013.
6) J. Golledge, R. M. Greenhalgh, and A. H. Davies: Stroke **31** (2000) 774.
7) M. V. McConnell, M. Aikawa, S. E. Maier, P. Ganz, P. Libby, and R. T. Lee: Arterioscler. Thromb. Vasc. Biol. **19** (1999) 1956.
8) B. N. Potkin, A. L. Bartorelli, J. M. Gessert, R. F. Neville, Y. Almagor, W. C. Roberts, and M. B. Leon: Circulation **81** (1990) 1575.
9) A. P. G. Hoeks, C. J. Ruissen, P. Hick, and R. S. Reneman: Ultrasound Med. Biol. **11** (1985) 51.
10) T. Länne, H. Stale, H. Bengtsson, D. Gustafsson, D. Bergqvist, B. Sonesson, H. Lecerof, and P. Dahl: Ultrasound Med. Biol. **18** (1992) 451.
11) P. J. Brands, A. P. G. Hoeks, M. C. Rutten, and R. S. Reneman: Ultrasound Med. Biol. **22** (1996) 895.
12) J. M. Meinders, P. J. Brands, J. M. Willigers, L. Kornet, and A. P. G. Hoeks: Ultrasound Med. Biol. **27** (2001) 785.
13) D. H. Bergel: J. Physiol. **156** (1961) 445.
14) L. H. Peterson, R. E. Jensen, and J. Parnel: Circ. Res. **8** (1960) 622.
15) K. Hayashi, H. Handa, S. Nagasawa, A. Okamura, and K. Moritake: J. Biomech. **13** (1980) 175.
16) H. Kanai, M. Sato, Y. Koiwa, and N. Chubachi: IEEE Trans. Ultrason. Ferroelectr. Freq. Control **43** (1996) 791.
17) H. Kanai, H. Hasegawa, N. Chubachi, Y. Koiwa, and M. Tanaka: IEEE Trans. Ultrason. Ferroelectr. Freq. Control **44** (1997) 752.
18) H. Hasegawa, H. Kanai, Y. Koiwa, and N. Chubachi: Electron. Lett. **33** (1997) 340.
19) H. Hasegawa, H. Kanai, and Y. Koiwa: Jpn. J. Appl. Phys. **41** (2002) 3563.
20) H. Kanai, Y. Koiwa, and J. Zhang: IEEE Trans. Ultrason. Ferroelectr. Freq. Control **46** (1999) 1229.
21) H. Kanai, H. Hasegawa, M. Ichiki, F. Tezuka, and Y. Koiwa: Circulation **107** (2003) 3018.
22) H. Hasegawa, H. Kanai, N. Hoshimiya, and Y. Koiwa: J. Med. Ultrason. **31** (2004) 81.
23) J. Inagaki, H. Hasegawa, H. Kanai, M. Ichiki, and F. Tezuka: Jpn. J. Appl. Phys. **44** (2005) 4593.
24) J. Inagaki, H. Hasegawa, H. Kanai, M. Ichiki, and F. Tezuka: Jpn. J. Appl. Phys. **44** (2006) 4732.
25) K. Tsuzuki, H. Hasegawa, H. Kanai, M. Ichiki, and F. Tezuka: Ultrasound Med. Biol. **34** (2008) 573.
26) H. Hasegawa and H. Kanai: IEEE Trans. Ultrason. Ferroelectr. Freq. Control **53** (2006) 2050.
27) S. P. Timoshenko and J. N. Goodier: *Theory of Elasticity* (McGraw-Hill, Tokyo, 1970).